Available online at www.sciencedirect.com

ScienceDirect

Procedia CIRP 94 (2020) 419–424

www.elsevier.com/locate/procedia

11th CIRP Conference on Photonic Technologies [LANE 2020] on September 7-10, 2020

Simultaneous *in operando* monitoring of keyhole depth and absorptance in laser processing of AISI 316 stainless steel at 200 kHz

Troy R. Allen[a]*, Brian J. Simonds[b], Jack R. Tanner[b], and James M. Fraser[a]

[a]*Queen's University, 64 Bader Lane, Kingston, Ontario K7L 3N6, Canada*
[b]*National Institute of Standards and Technology, 325 Broadway, Boulder, Colorado 80305, USA*

* Corresponding author. *E-mail address:* troy.allen@queensu.ca

Abstract

The formation of keyholes during high-irradiance laser-metal interaction is the complex, multiphysics phenomenon that underpins industrial processes such as laser-based additive manufacturing, laser welding, and laser cutting. The complex dynamics of energy coupling in keyhole formation are not well understood, and the energy absorptance in these processes are often assumed to be constant. Therefore, we implement two state-of-the-art measurement techniques *in operando* to simultaneously measure keyhole depth using inline coherent imaging and laser energy absorptance using integrating sphere radiometry at imaging rates of 200 kHz. Results directly reveal the time evolution of cavity-enhanced absorptance in these keyholes generated by the laser-metal interaction. For stationary irradiance on AISI 316 stainless steel, we find that processing in an argon-rich environment compared to air reduces coupling efficiency by 50 % ± 11 % in conduction, 27 % ± 2 % in transition, and 8 % ± 3 % in keyhole mode. High imaging rates allow clear observation of liquid surface oscillations and corresponding changes to absorptance, declining from 15 kHz to 10 kHz over the first 10 ms of the spot weld.

Keywords: laser welding; absorption; additive manufacturing; keyhole depth; *in operando* monitoring

1. Introduction

Laser welding, cutting, and additive manufacturing suffer from a lack of *in situ* monitoring tools and real-time control methods, leading to long development cycles for new processes, high rates of defects, and difficulty in setting industry standards [1, 2, 3, 4]. A crucial element of the laser-metal interaction that is often simulated but lacks experimental validation is the relationship between melt pool shape (including keyholes) and energy absorption [5, 6, 7, 8]. Recent efforts have made great progress on this problem through specialized research monitoring tools that directly image the melt pool and keyhole shapes (*i.e.*, high-speed x-ray imaging [9, 10]) and measure dynamic absorptance change (integrating sphere radiometry [11, 12]). Nevertheless, for purposes of modelling and predicting final part properties, absorptance is often measured pre-processing and treated as a static constant and melt pool/keyhole shape is simulated dynamically but only compared to post-mortem analysis. In this work, we combine inline coherent imaging (ICI), a tool designed to measure melt pool surface height/depth with micrometer precision at 200 kHz in industrial settings [13, 14, 15, 16], and integrating sphere radiometry (ISR), a tool able to measure absolute absorptance of laser power during the process at speeds up to 1 MHz [11, 17]. By observing both depth and absorptance at speeds faster than the system is changing, we can provide a clearer picture of how these intrinsically linked physical phenomena affect each other; thus, enabling the development of high-fidelity, deterministic models of the laser-metal processing system.

In this work, we apply this combined method to explore the effects of inert environments on the relationship between melt pool and keyhole depth and absorptance *in operando*. Argon

10.1016/j.procir.2020.09.157

cover-gas is regularly used in laser-metal processing applications to reduce oxidation induced defects at the liquid metal surface [18, 19]. We directly compare time-resolved melt pool and keyhole depth with absorptance data for spot welds performed in argon-rich atmosphere and air environments. Also presented is a comparison of the time-averaged data and a frequency analysis of the observed liquid surface oscillations.

2. Methods

2.1. Processing laser

High-irradiance stationary laser illumination is performed using a 1 kW Yb-doped fiber laser with a 100 µm core delivery fiber. A 150 mm focusing optic is used to focus the processing laser beam to a $1/e^2$ spot size of 238 µm. The focused beam has an M^2 value of 9.8 and a Rayleigh length of 4.23 mm. In this experiment, the laser is operated with powers ranging from 100 W to 410 W, confirmed to within 3 % with a commercial power meter. Pulse irradiance is calculated from the average power and the area of the beam incidence using the $1/e^2$ diameter. The laser is fired in pulsed mode to produce single pulses of 10 ms nominal duration. The actual pulse durations range from 9.896 ms to 9.972 ms depending on the laser power setting. The temporal distributions of the laser pulses are top hat in nature with rise times shorter than 75 µs.

2.2. Simultaneous inline coherent imaging and integrating sphere radiometry

ICI is low coherence interferometry implemented collinearly with the high-power processing beam [13, 14, 15, 16, 20]. The ICI system used in this work can extract sample height at a rate of 200 kHz, with an axial resolution of 15 µm (minimum axial distance between two interfaces that can be distinguished) and a single-point measurement repeatability of 0.6 µm. ISR is a technique that uses an integrating sphere to measure off-axis scattered light from laser illumination in order to calculate absolute absorptance [11, 17, 12]. The ISR system used in the present work measures scattered light in the sphere with a photodiode with a rise time of 4.4 µs. This system does not include a photodiode in the weld head, so absorptance from early in the welds, when reflections are primarily specular, are not reported in the figures (for durations after laser turn-on of up to 385 µs in air and 645 µs in argon). The influence of the vapor plume on integrating sphere-based absorptance measurements has been discussed in a previous work [12]. For the relatively short pulse durations and low irradiance values used in this work, the effect is expected to be negligible. ICI and ISR have previously been combined for simultaneous monitoring. Further description of the individual systems and the method for combining them can be found in Ref. [21].

2.3. Sample preparation

Samples of NIST SRM 1155a (AISI 316 stainless steel) [22] are prepared as described in Ref. [11]. Each SRM puck is polished to a consistent mirror-like finish and washed with methanol. NIST SRM 1155a was chosen for this experiment as there have been recent high-fidelity thermophysical property measurements into this system [23]. These improved measurements increase the accuracy of existing models, which when coupled with the proposed measurements allow for a more robust understanding of the keyhole dynamics during laser processing.

2.4. Processing in argon environment

For experiments involving an inert processing environment, modular gas flow ports on the integrating sphere are switched to allow it to be filled with argon. This experiment used 99.995 % industrial grade argon. Before each trial, the argon tank is opened and the flow rate into the sphere is monitored and kept low enough to ensure the position of the sphere is not disturbed. The gas flow is left on long enough to be confident that the full volume of the sphere has been recycled multiple times with argon gas. To remove any effect of the flow on melt pool behavior, it is shut off just before firing the laser pulse.

3. Results and Discussion

Single, stationary laser pulses of 10 ms each are applied to the NIST SRM samples, with a range of irradiance values encompassing conduction through keyhole mode (0.23 MW/cm^2 to 0.92 MW/cm^2). The ICI system performs one-dimensional depth measurements at a rate of 200 kHz with an axial resolution of 15 µm. ICI monitors the axial position of the metal surface at the center of the melt pool, which may be either a keyhole depth (positive value) or melt bead height (defined here as negative depth). This versatility which comes from its large depth of field and dynamic range, serves well for monitoring transition mode processing where it may need to track both behaviors at different times. Absolute absorptance of the processing laser energy by the metal sample is measured using ISR with a time resolution of 4.4 µs.

3.1. Dynamic depth and absorptance measurements in argon and in air

Figure 1 shows select time-resolved measurements of depth and absorptance from each processing regime (conduction, transition, and keyhole) and for processing in argon and in air. The zero point on the depth scale represents the position of the metal surface measured by ICI before the laser is turned on. Negative values for depth correspond to above the initial sample surface. Laser turn-on occurs at 0 ms.

First, considering conduction mode (Fig. 1 a-b), at 0.35 MW/cm^2, the most noticeable difference is the reduced absorptance under inert conditions. In both cases, the absorptance slowly rises with some rapid fluctuations, but in argon it plateaus to an average value of 0.21 and in air it rises to a maximum of 0.51. This difference is explained by reduced oxidation under inert conditions. This is consistent with the difference in appearance in the weld beads after processing. The welds performed in air were dark brown while in argon they were bright and shiny. Considerable difference is also seen in the depth measurements. In air, the center of the melt pool rises over time to a maximum height of 83 µm, with slight fluctuations throughout. In argon, the melt bead rises briefly before showing oscillatory behavior. In the figure, this appears as two distinct bands of data points around -25 µm and 20 µm.

In transition mode (Fig. 1 c-d), at 0.46 MW/cm^2, the behaviors in the two environments become more distinct. In air, we regularly observe the formation of temporary, highly volatile keyholes. These appear in the ICI data as sudden increases in depth, followed by rapid fluctuations, and eventually a sudden return to the pre-keyhole depth. Depth fluctuations are likely caused by sidewall protrusions or partial keyhole collapse, as both have the potential to limit the penetration of the ICI beam. The absorptance increases during these temporary keyholes to a maximum of 0.56, due to the temporary cavity formation. These shallow keyholes allow most of the processing light to interact with the workpiece multiple times due to reflections. It is interesting that even with the increased absorptance, the incident beam has sufficient energy to form a keyhole but not to sustain it. Surface tension pressure has been proposed as the likely cause for this behavior [24]. As irradiance increases through the transition mode in air (0.44 MW/cm^2 to 0.49 MW/cm^2), the frequency and duration of temporary keyholes increases until a consistent keyhole can be maintained [21]. In argon, it was possible to observe this behavior, albeit less frequently. More often, a keyhole would not form at all and instead the depth and absorptance would oscillate, similar to what was seen in conduction mode. This seemingly high variability between forming temporary keyholes or strong surface oscillations occurs over the narrow processing window from 0.45 MW/cm^2 to 0.52 MW/cm^2. The oscillating behavior is analyzed in greater detail in Section 3.3.

In keyhole mode (Fig. 1 e-f), at 0.58 MW/cm^2, the differences between air and argon conditions are reduced. For both environments, this irradiance is sufficient to quickly initiate keyhole formation and keep it open for the full 10 ms pulse. In argon, the keyhole growth rate is lower and does not reach the same maximum depth as in air for identical irradiances. The measured maximum absorptance is similarly reduced. These differences are expected, as oxygen content in assist gas has been shown to increase laser cutting speed [25] and improve the weldability of copper [26]. In both cases, an increase in initial absorptance due to oxidation was cited as the reason for these benefits. This claim seems to be confirmed by our data, as the weld in air has increased initial absorptance and greater achieved depths for the same laser exposure. Another effect that may play a part is the change in convective melt pool dynamics in inert environments. Specifically, the Marangoni flow is inward towards the center of the melt pool in the presence of high concentrations of oxygen and generally switches to outward flow when oxygen concentration is significantly reduced [27].

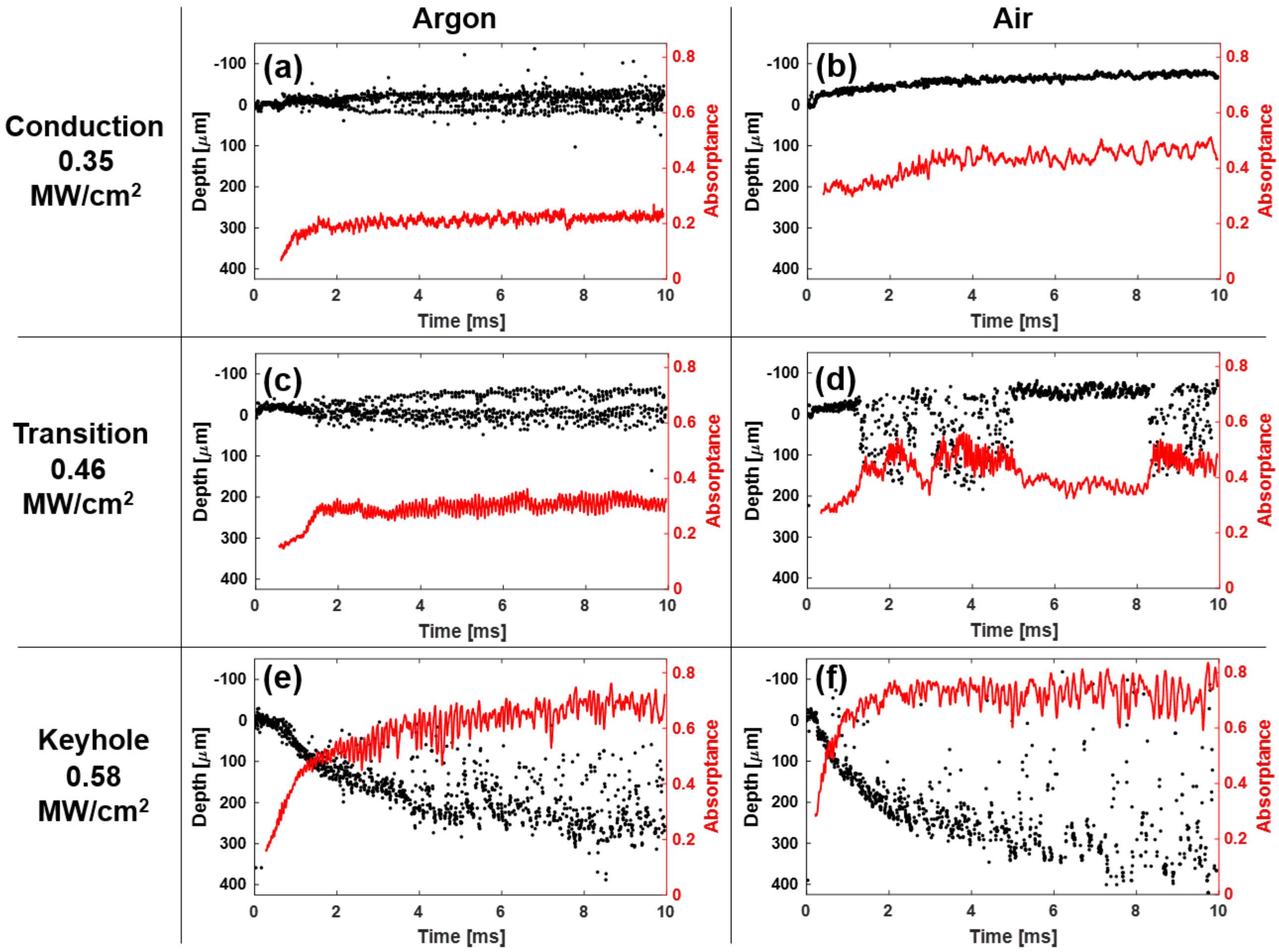

Fig. 1. Time-resolved depth and absorptance data from spot welds: **(a)** in argon at 0.35 MW/cm^2, **(b)** in air at 0.35 MW/cm^2, **(c)** in argon at 0.46 MW/cm^2, **(d)** in air at 0.46 MW/cm^2, **(e)** in argon at 0.58 MW/cm^2, **(f)** in air at 0.58 MW/cm^2.

3.2. Average depth and coupling efficiency in argon and in air

Time-averaged data, while only giving limited information about the dynamics of the process, are still useful for distinguishing thresholds between conduction and keyhole mode and for comparing general trends between processing parameters. From the time-resolved data shown in Section 3.1, it is straightforward to calculate the average absorptance (coupling efficiency) and average depth for each irradiance, as shown in Fig. 2.

For coupling efficiency, there is a striking gap at low irradiance due to lack of oxidation in inert environments. The largest difference is observed at an irradiance of 0.23 MW/cm^2, with argon and air environments giving coupling efficiencies of 0.08 and 0.42, respectively. As irradiance increases the argon coupling efficiency rises until the point where we start to observe temporary keyholes (the end of the conduction mode). In the absence of oxide formation this can be explained by the temperature dependence of absorptance [28, 29]. Over the same range in air, the measured coupling efficiency is relatively stable and even drops slightly before the transition mode starts, suggesting that oxide formation has a stronger influence than temperature on absorptance under these conditions. The slight drop may be caused by irradiance becoming high enough for oxide vaporization, but not yet high enough to generate sufficient recoil pressure to open a keyhole. Overall, conduction mode in argon compared to air has a 50 % ± 11 % reduction in coupling efficiency.

The main differences that occur in the transition regime between argon and air were described above alongside the time-resolved data, but here the difference in keyhole threshold is better displayed. At 0.45 MW/cm^2, both environments start to allow temporary keyholes to form. By 0.52 MW/cm^2, spot welds in air consistently form sustained keyholes. In argon, we do not observe this until 0.58 MW/cm^2. The coupling efficiencies measured at these thresholds are 0.58 for air and 0.59 for argon. These values are obviously similar, but also close to the expected Fresnel absorption value that one would obtain from two reflections off a liquid steel surface [30, 31, 8]. This may imply that regardless of processing conditions the start of keyhole mode is the formation of a shallow cavity that supports two reflections (*e.g.*, a cone with an aspect ratio of 1). This condition has been predicted in models for moving welds [32, 24].

In keyhole mode, the coupling efficiencies in both environments start to approach similar behavior. In this regime, factors that dominate absorptance in conduction and transition mode are now dwarfed by the geometric effects of keyholes and the multiple reflections they facilitate. Interestingly, the coupling efficiencies are closer than one would expect when considering that the argon spot welds have disproportionately lower average depth in this regime. Firstly, this may simply be because absorptance has a reduced sensitivity to depth as depth increases [6]. At a certain point, more reflections will have a negligible effect on the absorptance, so keyholes over a range of depths can all give similar absorptance. Another possibility is that the shape of the keyhole is generally different between the two environments, allowing the shallower keyholes in argon to give similar absorptance as those deeper ones in air. Regardless of the exact mechanisms, the coupling efficiency in keyhole mode in argon compared to air is reduced by only 8 % ± 3 %.

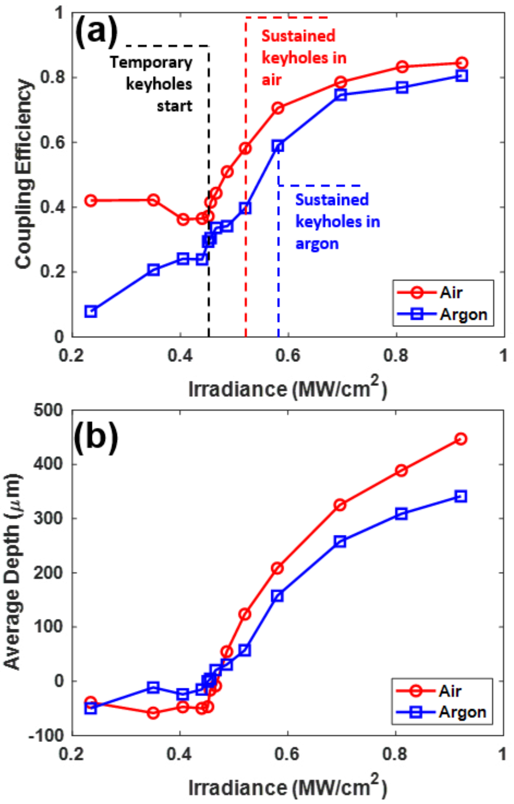

Fig. 2. Time-averaged data for **(a)** coupling efficiency and **(b)** average depth, for both argon and air environments.

3.3. Time-frequency data from transition mode in argon

Time-resolved data from the transition mode in argon suggests oscillatory behavior, but the relationship between frequency of depth and absorptance fluctuations is not obvious from simple inspection of Fig 1 c. We use a short-time Fourier transform (STFT) to quantify oscillation frequencies of the time-resolved depth and absorptance data and see how they evolve in time. STFTs cannot be performed on sparse data sets, and since ICI experiences occasional signal loss in this regime due to off-axis specular reflections, gaps in the depth measurements are linearly interpolated before frequency analysis. STFTs were performed on depth and absorptance data independently, using a Hann window with a length of 1 ms and 50 % overlap (to ensure equal sampling of all data points). Since absorptance data only starts at 0.57 ms (see Section 2.3) and because the pulse durations are not a full 10 ms, the STFTs exclude data from the first 1.07 ms and last 0.93 ms of the spot weld.

Figure 3 a-b show the results of STFTs performed on the time-resolved data in Fig. 1 c. In both the absorptance and depth spectrograms there is a distinct curve that starts near 15 kHz and decreases to 10 kHz over the weld duration. There are also fainter curves at multiples of these frequency values. These higher harmonics suggest that the oscillations are not perfectly sinusoidal. Also notable from the spectrograms is the width of the fundamental frequency peaks. These peaks are modeled well by Gaussian functions and all have full width at half

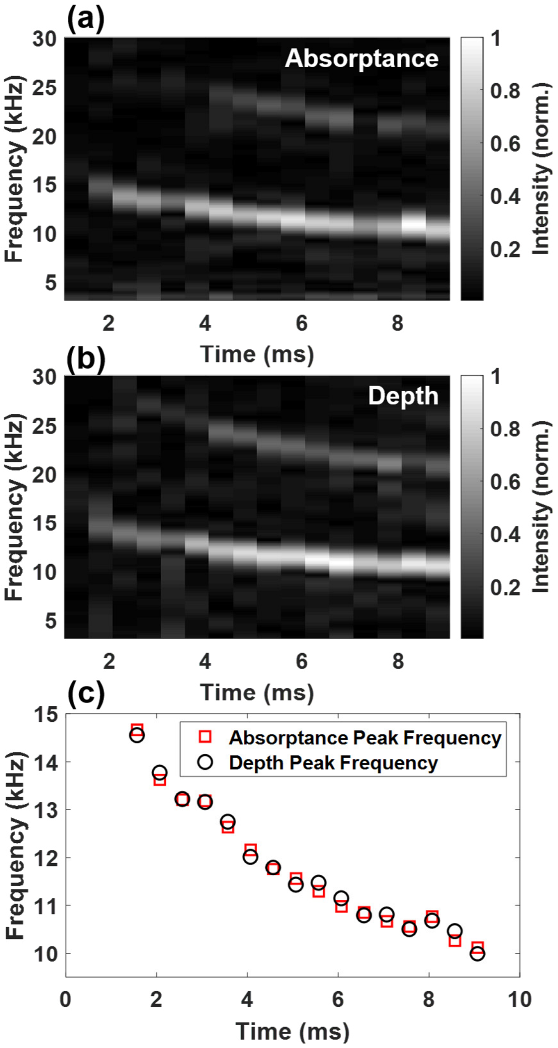

Fig. 3. Time-frequency data from a spot weld performed in argon environment at irradiance of 0.46 MW/cm^2. **(a)** and **(b)** show spectrograms generated by STFT for absorptance and depth, respectively. A Hann window was used with 1 ms length and 50 % overlap. Low frequencies (< 3 kHz) are excluded from the plot as they are not in a region of interest and contain DC noise. **(c)** Plot of the peak frequencies from each window of the STFTs found using Gaussian fits.

maximum close to 2 kHz. This gives a good estimate on the frequency resolution of this method, although the fit uncertainties on the center frequency positions are much lower (less than 10 Hz).

Figure 3 c plots the peak frequency (found by Gaussian fitting) as a function of time for both depth and absorptance. This shows more clearly how the fundamental frequency decreases over time, which is expected to occur as the melt pool volume grows [33]. The analogy of a vibrating drumhead is useful: a larger surface area drum has a lower resonance frequency. The second point is that the frequency of oscillations in depth and absorptance, which are measured independently, evolve together with similar values. This suggests that these non-keyhole surface oscillations are directly responsible for the oscillations in absorptance.

As mentioned in Section 3.1, we observe these strong surface oscillations throughout the transition mode in argon, but sometimes a repeated trial at the same irradiance will show temporary keyhole formation. Being so close to the threshold of keyhole formation, it is possible that the amplitude of the absorptance oscillations may dictate when these temporary keyholes form. As other work has shown, the fundamental frequency of the melt pool can be driven by modulating the laser beam at the same frequency to assist in laser drilling [34]. Here we show that driving these surface oscillations may not work only by mechanical resonance, but also by dynamic increases in energy coupling. This may open the possibility of fine control over keyhole formation (or suppression) by monitoring and exploiting surface mode oscillations.

4. Conclusion

By implementing ICI and ISR simultaneously to monitor laser spot welding of AISI 316 stainless steel, we have revealed unique insights into the underlying physics of laser-metal interaction. We showed that processing in argon compared to air significantly reduces coupling efficiency in conduction mode due to the lack of oxide formation. We observed that transition mode melt pools in argon undergo well-defined surface oscillations, decrease in frequency from 15 kHz to 10 kHz over time, and sometimes form temporary keyholes. These surface oscillations also produced highly correlated oscillations in absorptance. In a range of irradiance where sustainable keyholes could be formed, time-resolved and time-averaged data for spot welds in argon and in air become more similar, providing further evidence that multiple reflections is the dominant factor that influences absorptance in keyhole mode. These observations will be valuable for development of models and active control schemes, highlighting the importance of hybrid monitoring tools that measure multiple aspects of the process simultaneously.

Acknowledgements

The authors thank Chris Yung (NIST, Boulder), Nicholas Derimow (NIST, Boulder), and Norman Sanford (NIST, Boulder) for their careful reading of the manuscript and insightful comments. T.R.A. and J.M.F. acknowledge funding received from the Natural Sciences and Engineering Research Council of Canada, the Canadian Foundation for Innovation, and the Ontario Centres of Excellence.

References

[1] J. Svenungsson, I. Choquet and A. F. Kaplan, "Laser welding process – a review of keyhole welding modelling," *Physics Procedia*, vol. 78, pp. 182-191, 2015.

[2] B. Zhang, Y. Li and Q. Bai, "Defect formation mechanisms in selective laser melting: a review," *Chinese Journal of Mechanical Engineering,* vol. 30, no. 3, pp. 515-527, 2017.

[3] H. Bikas, P. Stavropoulos and G. Chryssolouris, "Additive manufacturing methods and modelling approaches: a critical review," *The International Journal of Advanced Manufacturing Technology,* vol. 83, pp. 389-405, 2016.

[4] M. Francois, A. Sun, W. King, N. Henson, D. Tourret, C. Bronkhorst, N. Carlson, C. Newman, T. Haut, J. Bakosi, J. Gibbs, V. Livescu, S. Vander Wiel, A. Clarke, M. Schraad, T. Blacker, H. Lim, T. Rodgers, S. Owen, F. Abdeljawad, J. Madison, A. Anderson, J.-L. Fattebert, R. Ferencz, N. Hodge, S. Khairallah and O. Walton, "Modeling of additive manufacturing processes for metals: Challenges and opportunities," *Current Opinion in Solid State and Materials Science,* vol. 21, no. 4, pp. 198-206, 2017.

[5] A. Kaplan, "A model of deep penetration laser welding based on calculation of the keyhole profile," *Journal of Physics D: Applied*

Physics, vol. 27, pp. 1805-1814, 1994.

[6] S. C. Wang and P. S. Wei, "Energy-Beam redistribution and absorption in a drilling or welding cavity," *Metallurgical Transactions B,* vol. 23, no. 4, pp. 505-511, 1992.

[7] C. Y. Ho and P. S. Wei, "Energy absorption in a conical cavity truncated by spherical cap subject to a focused high-intensity beam," *International Journal of Heat and Mass Transfer,* vol. 40, no. 8, pp. 1895-1905, 1997.

[8] W. Tan, N. S. Bailey and Y. C. Shin, "Investigation of keyhole plume and molten pool based on a three-dimensional dynamic model with sharp interface formulation," *Journal of Physics D: Applied Physics,* vol. 46, no. 5, p. 055501, 2013.

[9] R. Cunningham, C. Zhao, N. Parab, C. Kantzos, J. Pauza, K. Fezzaa, T. Sun and A. D. Rollett, "Keyhole threshold and morphology in laser melting revealed by ultrahigh-speed x-ray imaging," *Science,* vol. 363, no. 6429, pp. 849-852, 2019.

[10] A. A. Martin, N. P. Calta, J. A. Hammons, S. A. Khairallah, M. H. Nielsen, R. M. Shuttlesworth, N. Sinclair, M. J. Matthews, J. R. Jeffries, T. M. Willey and J. R. Lee, "Ultrafast dynamics of laser-metal interactions in additive manufacturing alloys captured by in situ X-ray imaging," *Materials Today Advances,* vol. 1, p. 100002, 2019.

[11] B. J. Simonds, J. Sowards, J. Hadler, E. Pfeif, B. Wilthan, J. Tanner, C. Harris, P. Williams and J. Lehman, "Time-resolved absorptance and melt pool dynamics during intense laser irradiation of a metal," *Physical Review Applied,* vol. 10, p. 044061, 2018.

[12] B. J. Simonds, E. J. Garboczi, T. A. Palmer and P. A. Williams, "Dynamic Laser Absorptance Measured in a Geometrically Characterized Stainless-Steel Powder Layer," *Physical Review Applied,* vol. 13, no. 2, pp. 024057, 2020.

[13] P. J. L. Webster, L. G. Wright, Y. Ji, C. M. Galbraith, A. W. Kinross, C. Van Vlack and J. M. Fraser, "Automatic laser welding and milling with in situ inline coherent imaging," *Optics Letters,* vol. 39, no. 21, pp. 6217-6220, 2014.

[14] J. J. Blecher, C. M. Galbraith, C. Van Vlack, T. A. Palmer, J. M. Fraser, P. J. L. Webster and T. DebRoy, "Real time monitoring of laser beam welding keyhole depth by laser interferometry," *Science and Technology of Welding and Joining,* vol. 19, no. 7, pp. 560-564, 2014.

[15] J. A. Kanko, A. P. Sibley and J. M. Fraser, "In situ morphology-based defect detection of selective laser melting through inline coherent imaging," *Journal of Materials Processing Technology,* vol. 231, pp. 488-500, 2016.

[16] T. G. Fleming, S. G. Nestor, T. R. Allen, M. A. Boukhaled, N. J. Smith and J. M. Fraser, "Tracking and controlling the morphology evolution of 3D powder-bed fusion in situ using inline coherent imaging," *Additive Manufacturing,* vol. 32, p. 100978, 2020.

[17] J. T. Norris, C. V. Robino, M. J. Perricone and D. A. Hirschfeld, "Development of a time-resolved energy absorption measurement technique for laser beam spot welds," *Welding Journal,* vol. 89, pp. 75-81, 2010.

[18] J. Xie and A. Kar, "Laser welding of thin sheet steel with surface oxidation," *Welding Journal,* vol. 78, pp. 343s-348s, 1999.

[19] C. L. A. Leung, S. Marussi, M. Towrie, R. C. Atwood, P. J. Withers and P. D. Lee, "The effect of powder oxidation on defect formation in laser additive manufacturing," *Acta Materialia,* vol. 166, 2019.

[20] P. J. DePond, G. Guss, S. Ly, N. P. Calta, D. Deane, S. Khairallah and M. J. Matthews, "In situ measurements of layer roughness during laser powder bed fusion additive manufacturing using low coherence scanning interferometry," *Materials & Design,* vol. 154, pp. 347-359, 2018.

[21] T. R. Allen, W. Huang, J. R. Tanner, W. Tan, J. M. Fraser and B. J. Simonds, "Energy coupling mechanisms revealed through simultaneous keyhole depth and absorptance measurements during laser-metal processing," *Physical Review Applied*, to be published.

[22] SRM 1155a., *AISI 316 Stainless Steel,* (National Institute of Standards and Technology; U.S. Department of Commerce, Gaithersburg, MD, 2013).

[23] P. Pichler, B. J. Simonds, J. W. Sowards and G. Pottlacher, "Measurements of thermophysical properties of solid and liquid NIST SRM 316L stainless steel," *Journal of Materials Science,* vol. 55, no. 9, pp. 4081-4093, 2019.

[24] R. Fabbro, "Depth dependence and keyhole stability at threshold, for different laser welding regimes," *Applied Sciences,* vol. 10, no. 4, p. 1487, 2020.

[25] H. Golnabi and M. Bahar, "Investigation of optimum condition in oxygen gas-assisted laser cutting," *Optics and Laser Technology,* vol. 41, no. 4, pp. 454-460, 2009.

[26] E. Biro, D. C. Weckman and Y. Zhou, "Pulsed Nd:YAG laser welding of copper using oxygenated assist gases," *Metallurgical and Materials Transactions A: Physical Metallurgy and Materials Science,* vol. 33, no. 7, pp. 2019-2030, 2002.

[27] C. Zhao, C. Kwakernaak, Y. Pan, I. Richardson, Z. Saldi, S. Kenjeres and C. Kleijn, "The effect of oxygen on transitional Marangoni flow in laser spot welding," *Acta Materialia,* vol. 58, no. 19, pp. 6345-6357, 2010.

[28] S. Boyden and Y. Zhang, "Temperature and wavelength-dependent spectral absorptivities of metallic materials in the infrared," *Journal of Thermophysics and Heat Transfer,* vol. 20, no. 1, pp. 9-15, 2006.

[29] T. J. Wieting and J. L. Derosa, "Effects of surface condition on the infrared absorptivity of 304 stainless steel," *Journal of Applied Physics,* vol. 50, no. 2, pp. 1071-1078, 1979.

[30] W. Schulz, G. Simon, H. M. Urbassek and I. Decker, "On laser fusion cutting of metals," *Journal of Physics D: Applied Physics,* vol. 20, no. 4, pp. 481-488, 1987.

[31] R. Ducharme, K. Williams, P. Kapadia, J. Dowden, B. Steen and M. Glowacki, "The laser welding of thin metal sheets: an integrated keyhole and weld pool model with supporting experiments," *Journal of Physics D: Applied Physics,* vol. 27, pp. 1619-1627, 1994.

[32] V. Semak and A. Matsunawa, "The role of recoil pressure in energy balance during laser materials processing," *Journal of Physics D: Applied Physics,* vol. 30, no. 18, pp. 2541-2552, 1997.

[33] Y. H. Xiao and G. Den Ouden, "A study of GTA weld pool oscillation," *Welding Journal,* vol. 69, pp. 289s-293s, 1990.

[34] S. Ly, G. Guss, A. M. Rubenchik, W. J. Keller, N. Shen, R. A. Negres and J. Bude, "Resonance excitation of surface capillary waves to enhance material removal for laser material processing," *Scientific Reports,* vol. 9, no. 1, pp. 1-9, 2019.